A space domain energetics study for CO2 increasing based on SRES-A2 emission scenario

Advances in Meteorology, New York, v. 2013, p. ID697105/1-ID697105/19, 2013
http://www.producao.usp.br/handle/BDPI/44729

Hindawi Publishing Corporation
Advances in Meteorology
Volume 2013, Article ID 697105, 19 pages
http://dx.doi.org/10.1155/2013/697105

Research Article

A Space Domain Energetics Study for CO_2 Increasing Based on SRES-A2 Emission Scenario

José Augusto P. Veiga,[1,2] Tercio Ambrizzi,[2] and Alexandre B. Pezza[3]

[1] *Institute of Technology, Amazon State University, Avenida Darcy Vargas 1200, 69065-020 Manaus, Brazil*
[2] *Institute of Astronomy, Geophysics and Atmospheric Sciences, University of São Paulo, São Paulo, Brazil*
[3] *School of Earth Sciences, The University of Melbourne, VIC, Australia*

Correspondence should be addressed to José Augusto P. Veiga; veiga.uea@gmail.com

Received 1 July 2013; Revised 30 September 2013; Accepted 1 October 2013

Academic Editor: Anthony R. Lupo

This work presents a detailed investigation of the changes in the global pattern of energetics under a prescribed temporal evolution of CO_2 concentration as proposed by the A2 IPCC forcing scenario (SRES-A2) using a combination of reanalysis and climate models. A validation climatology is computed using the classic Lorenz energetic formulation, with generation and dissipation components estimated as residuals. The results show a good agreement overall between models and reanalysis for the present day climate, noting that the models generally give more zonal energy and less eddy energy when compared to the reanalysis. Spatial analysis translates the above results as models depicting greater energy associated with the subtropical jet streams than effectively observed. This pattern is observed regardless of season or hemisphere. The projections for future climate scenarios suggest a further increase in the zonal kinetic energy, with a slight average reduction in all other terms. This pattern is seen in association with a substantial decrease in the conversion term mainly associated with sensible heat transport (CA) under a warmer climate. In agreement with recent work in the literature, our results suggest an overall reduction of the global energetics under increasing CO_2.

1. Introduction

Recent studies have shown that the tendency for planetary temperature increase observed in the 20th century has caused a global change on the earth-atmosphere energy balance and consequently altered the atmospheric disturbances behavior in a broad range of spatial and temporal scales. The cause of the changes has been majorly attributed to a gradual and continued increase of greenhouse gas emissions to the atmosphere [1–3]. According to the fourth IPCC report [4], the fossil fuel burning process, demanded by the human energy consumption, land use, and agricultural activities are anthropogenic components responsible for the CO_2 concentration increasing, as well as NH_4 and N_2O (hereafter called GHGs). The rising of the GHGs atmospheric concentration amplifies the greenhouse effect efficiency by trapping more heat in the atmosphere, and as a consequence the atmosphere has its circulation pattern altered and adjusted to the additional heating as to establish a new equilibrium condition. However, the consequences for the atmospheric circulation patterns can be felt trough the changes in a broad spatial and temporal scale of eddy disturbances. For example, the author in [1] investigated the linear relation between the frequency of cyclones and anticyclones with the Northern Hemisphere (NH) continental surface temperature and showed a direct relation between both; that is, in the period of increasing (decreasing) surface air temperature the number of registered cyclones diminished (rose). The authors in [5] observed an increase in the number of cyclone cases at high latitudes and a falling in their frequency at middle latitude zones for boreal winter in the period of 1966–1993. According to the authors, the poleward displacement of the baroclinic zone has increased the number of cyclones at higher latitudes and diminished their frequency in the middle latitudes. The

authors affirmed that the rising of CO_2 concentration in the atmosphere has influenced the migration of the baroclinic zone to the north and consequently caused a reduction in the number of cyclones in middle latitudes followed by the rising frequency of disturbances at higher latitudes.

Similar results were found by the authors in [6] who observed a tendency of rising (decreasing) in the number of cyclone cases in high (middle) latitude regions for the winter season. However, the authors noted, for the period of analysis 1959–1997, a positive tendency in the number of strong cyclones in both mid and high latitudes. The authors in [2] observed an increase in the number of intense cyclone cases in the north Atlantic and north Pacific and in the Eurasia continent. Although the number of strong cyclones has been observed to increase in those regions, the total number of cyclones, including the less intense cases, remained unchanged. Based on idealized simulations with moist static stability parameter, the author in [7] has found that extratropical kinetic energy is reduced in a warmed climate and the length of extratropical systems depends on the strength of the warming. For the Southern Hemisphere (SH), studies have shown similar tendencies of frequency and intensity of cyclones [8–11]. However, the authors in [12] bring into attention the important fact of using cyclone detection and tracking algorithms to determine the frequency and life cycle of extratropical cyclones. According to them, due to a range of different characteristics related to the cyclones formation, their asymmetry and life cycle can differ from each other and result in different diagnostics [13]. One of their main results suggests that, after the differences between the tracking schemes, the number of weaker systems is reduced under increasing greenhouse gas forcing, while the number of stronger systems rises in specific areas of the Northern Hemisphere during winter seasons. Tropical cyclones are another range of atmospheric disturbances that can be potentially affected by global warming [14–17].

This study focuses on the atmospheric energetics response to a higher greenhouse gas concentration, as prescribed by the SRES-A2 forcing [4], using three coarse-resolution coupled atmosphere-ocean models. There are several ways to formally study the impact of a warmer environment on the energy cycle, as those used in the studies of [18–23]. In the present work, we focus on the changes in the main energy terms: available potential and kinetic energy, and their conversions for the SRES-A2 forcing, using a formulation in which, different from previous studies [18], the eddy component is taken as the direct calculation of the differences from the zonal mean. The Lorenz energy cycle is a robust way to estimate how the available potential energy is produced and converted into zonal and eddy kinetic energy via barotropic and baroclinic conversions.

Recently, the literature has started to address the question of how the energy will respond to global warming in a more formal sense. This was brought to light particularly by the work of the author in [24]. In this work the authors used an approach based on the formal Eulerian mean decomposition, where the energetics is also given in terms of calculations in the transient which runs over a 10-year run with 3% increase in CO_2. In this way, the authors obtained an empirical (fictitious) distribution which provides an estimate of the variability of the energy terms under increased CO_2 scenarios. While the author in [24] conclude that there is a reduction in the strength of the Lorenz energy cycle with an increase in zonal mean kinetic energy due to global warming in one model, here we show a further global variability in three different models compared to the European and American Reanalyses.

2. Data and Methodology

2.1. Reanalysis and Coupled Climate Model Data. Data of horizontal wind components (zonal and meridional), air temperature, omega vertical velocity, and geopotential height from two reanalysis projects and from three national research centers were used to compute the global energetics in the space domain. The energy analysis is carried out for two distinct periods. The first is from 1979 to 1999 and the second is between 2079 and 2099. The National Center for Environmental Prediction (NCEP/NCAR Reanalysis 2) [25] and the European Centre for Medium-Range Weather Forecasts (ERA-40) [26] data are 2.5×2.5 regularly grid spaced. These data were obtained, respectively, from the NOAA-CIRES Climate Diagnostic Center available on the website http://www.cdc.noaa.gov/ and http://www.ecmwf.int/. The coupled climate global models are the ECHAM5, developed by the Max Planck Institute for Meteorology [27], CGCM3, developed at the Canadian Centre for Climate Modelling and Analysis [28], and the third version of the ocean-atmosphere model initially developed at the Centre European de Recherche et de Formation Avancée en Calcul Scientifique (CERFACS) then regularly updated at the Center National Weather Research, CRNM [29]. Data from the coupled climate models used in this study present varying horizontal resolution. Data from ECHAM5 has a spatial resolution equivalent to $1.875^\circ \times 1.875^\circ$ degrees, as the model runs with a horizontal resolution of 63 waves triangular spectral truncated and 31 levels in the vertical (T63L31). The CGCM3 atmospheric components were run with a horizontal resolution of 47 waves triangular spectral truncated and 31 levels in the vertical (T47L31), which is equivalent to $3.75^\circ \times 3.75^\circ$ degrees. The CRNM global coupled climate model runs with a horizontal resolution of 42 waves triangular spectral truncated and 45 levels in the vertical (T42L45), which is equivalent to a horizontal resolution of $2.8^\circ \times 2.8^\circ$ degrees. The atmospheric variables were integrated from the lowest level, considered to be at the surface (1000 hPa) up to 100 hPa. The atmospheric energetic terms determined for each model and reanalysis datasets include zonal and perturbed available potential energy and kinetic energy, generation of available potential energy, conversion terms, and dissipation of kinetic energy terms.

The CMIP3 models were the natural choice for this work because they have already been sufficiently studied and validated as to be able to compare our results with those of previous works employing similar energetics techniques. We also note that the recent literature suggests that the CMIP5

models contain very similar biases as the CMIP3 runs over the Pacific Ocean (Damien Irving, manuscript under review).

2.2. Space Domain Energetics Method. A traditional and compact form of presenting energy computations is suggested by Lorenz [18], where the potential energy, which is available to be converted into kinetic energy, can be split into zonal available potential energy (AZ), the energy associated with the zonal averaged state, and eddy available potential energy (AE), the energy related to the departure from the zonal mean state. The kinetic energy can be treated similarly as potential energy; that is, the kinetic energy of the flow can be separated into its zonal (KZ) and eddy (KE) parts. From a four-component view the spatial domain Lorenz energy cycle (SDLEC) can be written as

$$\frac{\partial \mathrm{AZ}}{\partial t} = -\mathrm{CZ} - \mathrm{CA} + \mathrm{GZ}, \tag{1}$$

$$\frac{\partial \mathrm{AE}}{\partial t} = \mathrm{CA} - \mathrm{CE} + \mathrm{GE}, \tag{2}$$

$$\frac{\partial \mathrm{KZ}}{\partial t} = \mathrm{CK} + \mathrm{CZ} - \mathrm{RKZ}, \tag{3}$$

$$\frac{\partial \mathrm{KE}}{\partial t} = \mathrm{CE} - \mathrm{CK} - \mathrm{RKE}. \tag{4}$$

The last term in (3) and (4) can be combined and computed in the form of residuals, with the incorporation of calculation errors related to the time derivatives (εKZ and εKE) in the form

$$\mathrm{RKZ} = \mathrm{DZ} + \varepsilon\mathrm{KZ}, \tag{5}$$

$$\mathrm{RKE} = \mathrm{DE} + \varepsilon\mathrm{KE}. \tag{6}$$

The conversion terms are labeled as CZ, CA, CE, and CK, respectively, denoting the conversion from AZ into KZ, AZ into AE, AE into KE, and KE into KZ. The CZ term depends upon the covariance between zonal means of vertical velocity and temperature. CZ reflects the growth of KZ at the expense of AZ when there is warm air rising and cold air sinking latitudinally. The CA term depends upon the relation between the meridional transport of sensible heat and the meridional gradient of zonal averaged temperature, and the vertical transport of sensible heat and the vertical gradient of zonal averaged temperature.

The CE term depends upon the covariance between the departure from the mean value (eddy) of vertical velocity and temperature. According to this conversion, the term KE increases at the expense of AE when warm air rises and cold air sinks longitudinally. These three forms of energy quantities are known as baroclinic conversions as they are related to heat transport. The CK term, named as barotropic term, depends upon the horizontal (zonal and meridional) and vertical transport of angular momentum. For instance, if CZ is positive (negative), there is local growth of KZ (AZ) at the expense of AZ (KZ). Generation of AZ (AE) occurs when there is meridional (zonal) differential heating.

Detailed mathematical expressions for all the components of the energy budget, as described by (5) and (6) are presented in the appendix. Here the Lorenz diagram considers that the conversion terms are always positive, with the arrows indicating the direction of the fluxes. The rates of generation of available potential energy and dissipation of kinetic energy are obtained here as residuals as these rates are difficult to calculate directly.

It is now convenient to explain the main differences between the methodology applied in this study and those used in [30–32]. In these papers all the reservoirs and conversion terms involve first- and second-order climate statistics (means, variance, and covariance) of the basic prognostic variables [30]. They include in the calculus of energetics the participation of standing and transient eddies, respectively, related to zonal and time differences. However, the energetics methodology applied in this study takes into account the eddy as the difference from the zonal mean or the standing eddies. Following this methodology, there are some differences between the results of this work and those previously mentioned, especially for meridional energy distributions. However, in a volume integrated sense both techniques show similar and coherent values that suggest that both forms of analysis are robust when global energetics is considered. We further note that caution should be taken when comparing the integrated values shown by several authors, especially because of the different range of vertical integration of each work. Rather, it is the orders of magnitude and the proportion amongst each energy terms which give the most meaningful interpretation.

3. Results

3.1. Time Series of Energy and Conversion Terms. In [33], the authors validate five models against the energetics, using an approach based on wave spectra decomposition to study the potential effects of global warming on the energy cascade feedback-loop in the atmosphere. They showed that most of the models simulate reasonably well the energy wave spectra and the downscale energy cascade as well as the energy transfer for the zonal wave interactions of kinetic energy, but with generally too much energy in the models. As we will see, our validation results show a similar behaviour in terms of global averages with additional nuances, as we also explore the behaviour of the generation terms. For instance, the eddy available potential energy is generally weaker in the models compared to the reanalyses during the northern winter, suggesting a smaller potential for transient disturbances to form. In connection to that of this pattern, the models also have a more positive global average generation of KE compared to that of the reanalysis (regardless of magnitude), where this term is usually negative. As we will discuss in this section, this behaviour suggests a lesser ability of models in generating transient disturbances in the atmosphere when compared to the reanalyses, at least for the Northern Hemisphere, regardless of potential impacts of global warming.

Firstly, time series of generation, available potential energy, and kinetic energy for their zonal and eddy components are compared for the reanalysis (ERA-40 and NCEP-II) and coupled models (CNRM, CGCM3, and ECHAM5)

Figure 1: Climatological annual cycle of the generation of zonal available potential energy (a), generation of eddy available potential energy (b), zonal available potential energy (c), eddy available potential energy (d), zonal kinetic energy (e), eddy kinetic energy (f), dissipation of KZ (g), and dissipation of KE (h) for the period from 1979 to 1999. Standard units are 10^5 Jm^{-2} for energy terms and Wm^{-2} for generation and dissipation terms.

datasets. The mean values of each term were calculated by integrating the atmosphere globally from the surface up to 100 hPa. Hereafter, the northern winter and summer represent the period from December through February (DJF) and June to August (JJA). The climatological annual cycles of generation, available potential energy, and kinetic energy, with their zonal and eddy parts, from the reanalysis and coupled models are illustrated in Figure 1. The values of GZ for the reanalysis are maximized from January to March (Figure 1(a)), while GE highest values are observed

in winter months (Figure 1(b)). The coupled climate models overestimate GE and do not produce the maximum negative values of GE as observed in reanalysis. This is suggestive of more energy to be converted into KE in the case of coupled models. The opposite behavior is observed in the case of GZ, where coupled models usually underestimate the reanalysis. A comparison between coupled models and reanalysis shows that their results are climatologically similar. Zonal available potential energy (Figure 1(c)) presents a small variation around the year relative to the eddy component (Figure 1(d)). An important aspect concerns the maximization of AZ and minimization of AE by the coupled models relative to reanalysis. The major discrepancy between both data sets is observed for the values of AE. A smaller production of AE by the coupled models can be reflected into the growing of eddy disturbances via baroclinic processes and/or a redirection of energy to GE and AZ terms. The greater input of AZ by the coupled models can yield stronger jet streams, comparatively to that produced with reanalysis. The maximum values of KZ from the coupled models can be observed from Figure 1(e). With exception of the CNRM model, for autumn and summer all other models overestimate KZ, with CGCM3 producing the highest values. A positive aspect is that all the models follow the reanalysis climatological annual cycle. The highest values of KE from the coupled models, especially those observed from ECHAM5, suggest that the kinetic energy related to the disturbances may be stronger than the reanalysis but not on a consistent basis, depending on the model. Dissipations of KZ and KE (Figures 1(g) and 1(h)), determined as residual, are well produced by the coupled models.

Figure 2 illustrates the time series for energy conversions determined by both reanalysis and coupled models. According to the reanalysis data sets, CZ, which is responsible for the connection between AZ and KZ with a natural energy flow in the direction of KZ by the zonal-mass overturning circulation, presents maximum values during the NH summer months (Figure 2(a)). The models adequately produced this maximum, though the CGCM3 model underestimates CZ and the ECHAM5 and CNRM yield values higher than those of the reanalysis. An important point is that climatologically CZ is always positive which corroborates the natural growing of KZ at the expense of AZ. The connection between the available potential energies is made by CA and the results of this conversion term are illustrated in Figure 2(b). The energy supply from AZ to AE or vice versa depends on the balance between meridional and vertical heat transfer, with a growing of AE when the result is positive. In this case, it can be noted that CA is always positive which is indicative of an energy flow from AZ to AE in both reanalysis and coupled models at high latitudes during the winter hemisphere. Furthermore, both reanalysis values are very similar, and their phase and amplitude are strongly locked around the year. Models do produce adequately the positive values of CA and its climatological annual cycle when compared with reanalysis. Maximum values of CA are observed during winter months, followed by a flat curve for summer months where the baroclinic instability is greatly reduced. Figure 2(c) shows the behavior of annual cycle of CE. It can be noted that both reanalyses produce similar values of CE, including their seasonality, whereas the values of CE relative to the coupled models are more dispersive and in some cases they are out of phase (for instance, CNRM and ECHAM5). Positive values of CE are indicative of the growing of disturbances by baroclinic processes at the expense of AE. This conversion is stronger during both summer and winter, followed by a minor conversion, but still in the direction of growing KE, during transition seasons. In this context, all the models overestimate the values of such conversion when compared with both reanalyses meaning that they are able to produce stronger disturbances than the reanalysis. Once the disturbance grows, they can transfer energy to either zonal flow or minor scale disturbances via dissipative processes. The way the energy is converted to intensify zonal flows can be detected by CK: when it is positive KZ grows at the expense of KE by barotropic processes, that is, by momentum transfer. Figure 2(d) illustrates the annual cycle of CK. A good similarity between both reanalyses and models can be seen. The models reproduce month to month variations well and their values are very similar to those of the reanalysis, except the ECHAM5 which overestimates both negative and positive values of CK from reanalysis, respectively, for January to March and May through September. Although CK presents low values compared to the other conversion terms they still indicate important global features associated with barotropic process such as blocking. For JJA, KZ grows at the expense of disturbances, while the disturbances grow at the expense of KZ for DJF.

3.2. Latitudinal Distributions of the Energy Components. The energy analysis previously discussed is related to the time variation of a global integration with implicitly meridional and vertical contributions to energy and conversion terms. However, a detailed view into the latitudinal distribution of the Lorenz energy components is necessary to clarify important aspects relative to the differences between coupled models and reanalysis energetics. The meridional distribution of available potential energy and kinetic energy terms for both data sets during the NH winter and summer is illustrated in Figure 3. The results show high values of zonal available potential energy from high latitudes until ~45°S followed by two minor peaks of AZ around equatorial and middle latitudes in the NH (Figure 3(a)). The results from coupled models show that they can reproduce reasonably well both the phase and amplitude of AZ values. Most differences are observed in the high SH latitudes where ECHAM5 underestimates the values of AZ and the CGCM3 overestimates it at NH mid latitudes. According to [30], high values of AZ in high latitudes are due to the low values of temperature in the high troposphere produced by the models. The results for AZ during summer are opposite in the winter season (Figure 3(b)). In this season, NH high latitudes present the highest values of AZ when compared to others locations, including the SH. For this season the results from the models show good similarities in comparison with those from the reanalysis. Significant differences between reanalysis and coupled models relative to the production of zonal kinetic

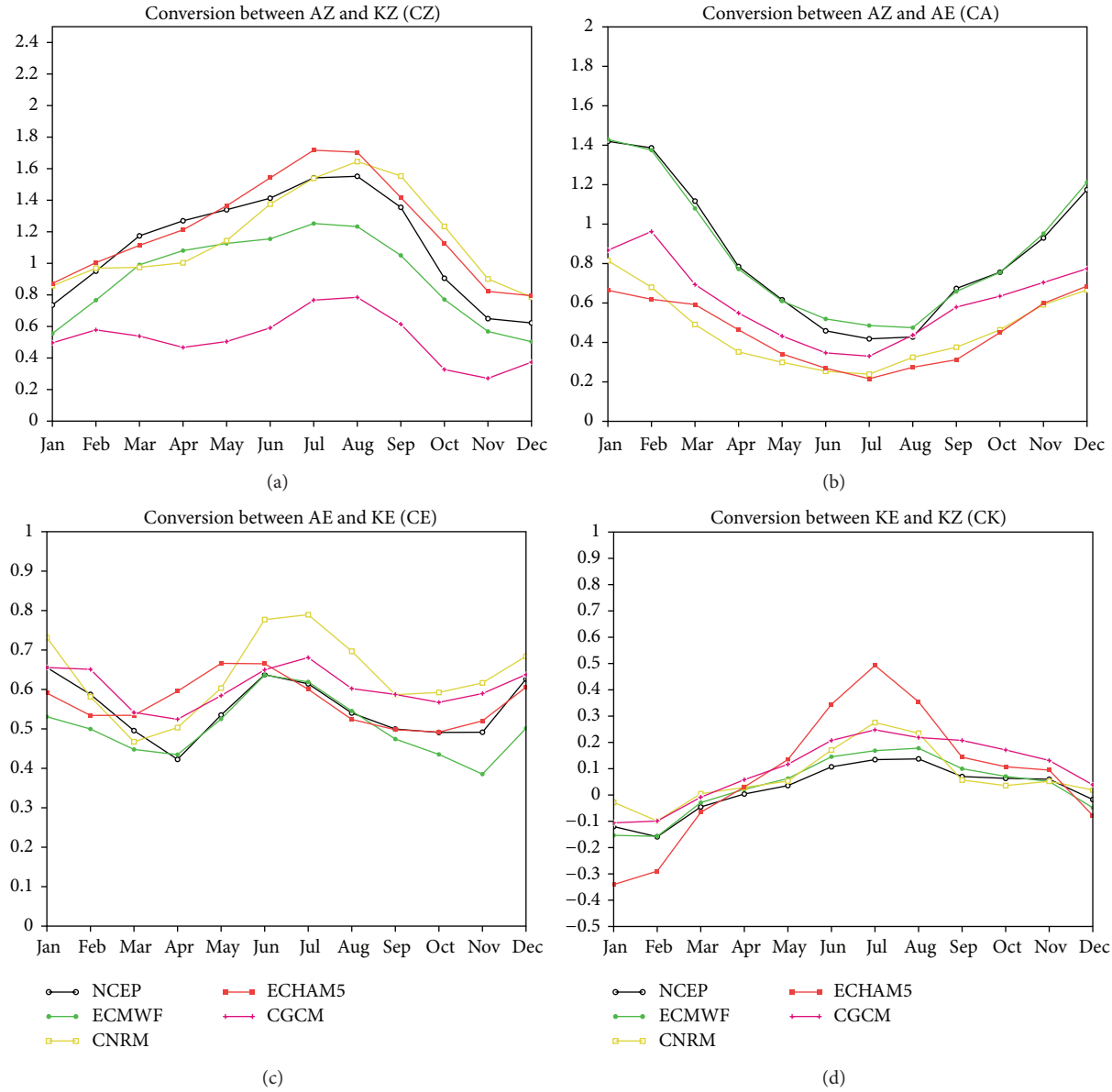

Figure 2: Climatological annual cycle of the conversion between AZ and KZ (a), conversion between AZ and AE (b), conversion between AE and KE (c), and conversion between KE and KZ (d) for the period between 1979 and 1999. Units are Wm^{-2}.

energy are seen from Figures 3(c) and 3(d). Excessive zonal mean kinetic energy in the coupled models is observed in SH and NH for the winter season. The models almost duplicate the values of KZ in the SH and overestimate KZ in the NH, except for the CGCM3 which produces values of KZ similar to those of both reanalyses. During JJA the reanalyses show the double jet structure associated with the subtropical jet stream and polar frontal jet (Figure 3(d)). ECHAM5 and CNRM seem to miss these features and shift the jet core to lower latitudes. The eddy available potential energy for both seasons is depicted in Figures 4(a) and 4(b). It can be seen that the value of KE for coupled models is consistently lower than that from both reanalyses during winter months. The peak of AE during this month is observed to be just of 60°N (Figure 4(a)). For summer months, the values of AE are relatively lower and flatter than in winter, with coupled models underestimating AE when compared with the reanalysis (Figure 4(b)). Eddy kinetic energy during winter season presents maximum values north of 60°N (Figure 4(c)). The coupled models underestimate the values of KE in high latitudes in the NH; however, they are able to reproduce the flat and low values observed in the SH. In particular, coupled models produce excessive KE in the tropics during summer when compared to reanalysis, as observed from Figure 4(d). This can be interpreted as the disturbances formed in the region where KE is considered; for instance, in the case of the tropics there is tropical disturbances formation. Furthermore, at this time, it is not possible to infer what kind of disturbance

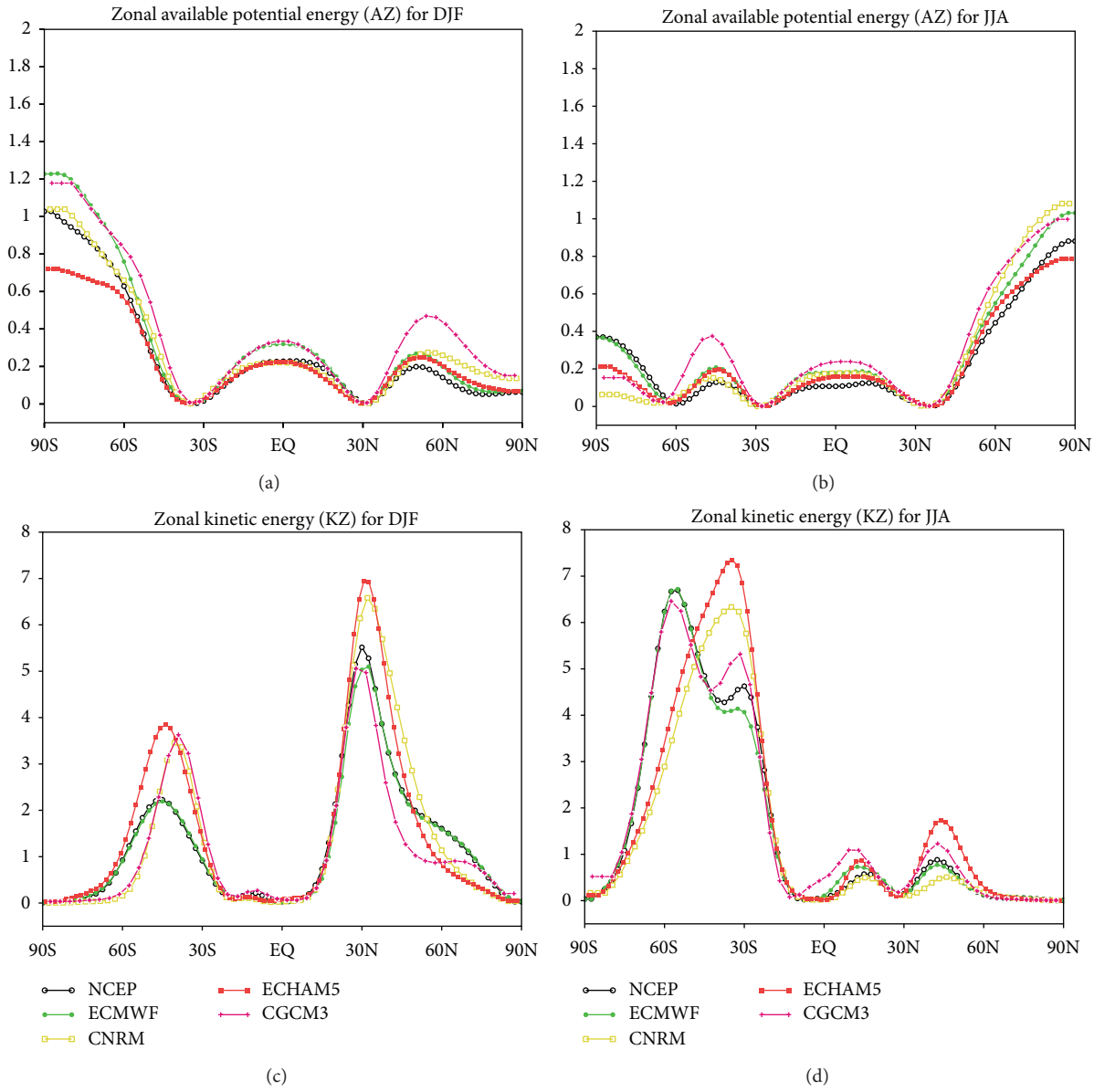

Figure 3: Latitudinal distribution of volume integrated zonal available potential energy for DJF (a) and JJA (b) and zonal kinetic energy for DJF (c) and JJA (d) for the period from 1979 to 1999. Units are 10^5 Jm^{-2}.

is related to KE quantities. To better evaluate such attribution, a regional energy quantification should be carried out using a fine grid resolution data, which is beyond the scope of this study. Similar results for AE and KE were found in [26] in which the authors applied a global energetic study for the last glacial maximum climate. In this study they split the energy components into transient and stationary eddies. The conversion terms in the Lorenz energetic explain how the energy flows from one kind of energy into another, as a response to the dynamical behavior of the atmosphere. To detail the geography of the conversions, based on vertical integrands around latitudinal positions, Figure 5 is presented. There is little difference between the values of CZ produced by the NCEP reanalysis (Figure 5(a)), especially in the equatorial region for DJF. Such small difference is not observed to occur in ECMWF reanalysis. As this term is relative to the flow of energy between AZ and KZ, where positive values mean a growth of KZ by the mass overturning due to meridional heat differences in the atmosphere, it can be seen from the reanalysis that there are maximum negative values around mid latitudes in the NH followed by a maximum at 60°N. The models are able to yield these peaks and the general latitudinal variance of CZ. The maximum values of CZ in the NH are coincident with maximum of KZ in the same region (Figure 5(a)). This is theoretically true, as KZ grows at the expense of available potential energy when CZ is positive. During summer months (Figure 5(b)) the values of CZ present a higher regional variability and

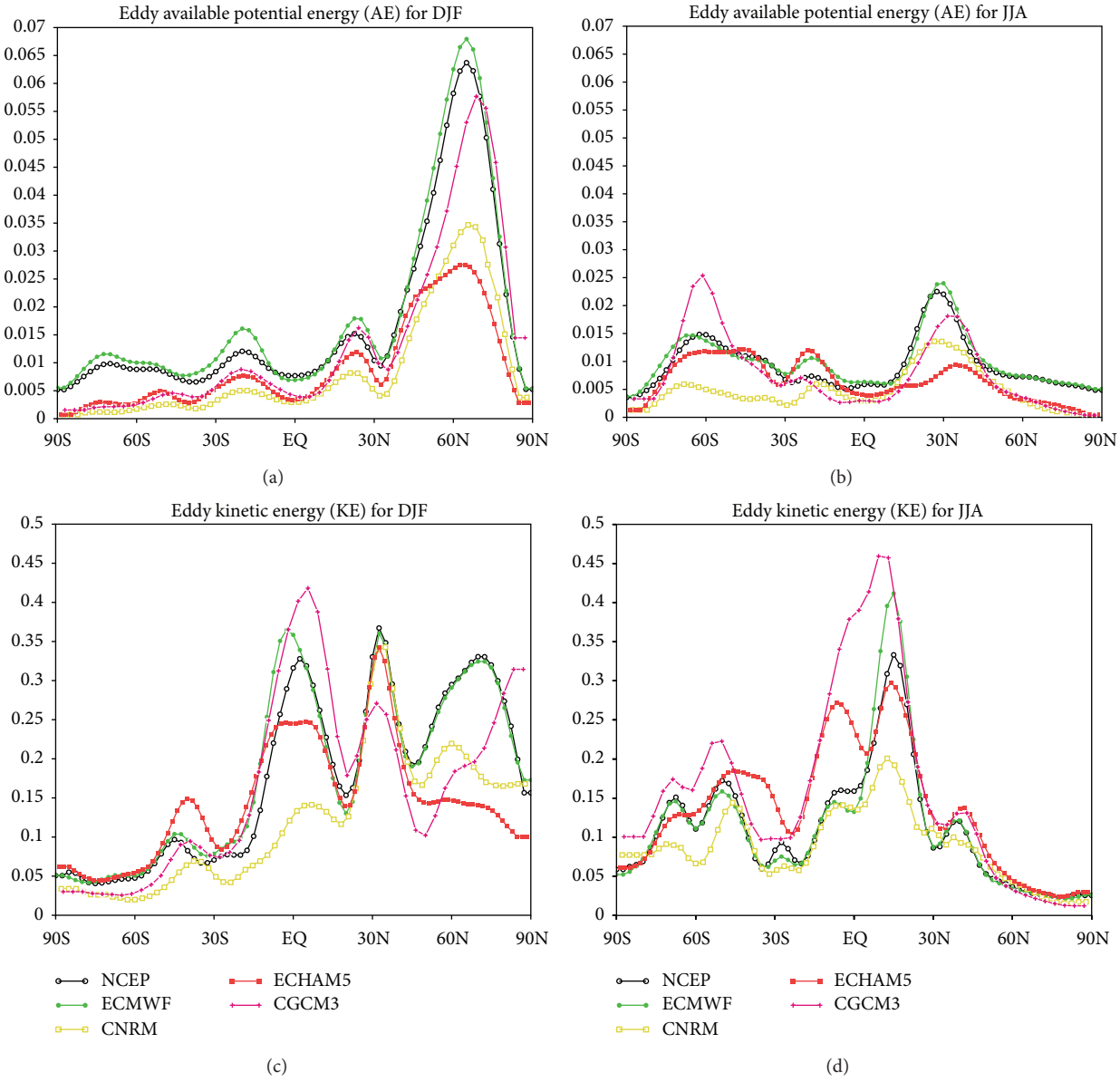

Figure 4: Latitudinal distribution of volume integrated conversion between AZ and KZ (CZ) for DJF (a) and JJA (b), conversion between AZ and AE (CA) for DJF (c) and JJA (d), conversion between AE and KE (CE) for DJF (e) and JJA (f), and conversion between KE and KZ (CK) for DJF (g) and JJA (h) averaged for the period from 1979 to 1999. Units are Wm^{-2}.

apparently less coherence. Figure 5(c) depicts the latitudinal distribution of CA for winter months related to reanalysis and coupled models. There is a good agreement in phase and amplitude. Most values of CA are positive which is indicative of increasing AE at the expense of AZ by the process of sensible heat transfer crossing different latitudes. According to these results around mid and high latitudes in the NH AZ feeds AE and KE grows at the expense of AE (Figure 5(e)) by baroclinic processes, which explains the well-known formation of transient disturbances via baroclinic instability. The same process occurs in the SH as seen by Figures 5(d)–5(f) during JJA, however, with less intensity. Values of CA for the SH during DJF are flat when compared to those of the opposite season, with maximum positives around 60°S. Figure 5(g) shows that both models and reanalyses produce negative values of barotropic conversion (CK) during DJF in low latitudes. Negative values of CK imply the growth of eddies at the expense of the mean zonal flow at this particular region. Coupled models produce similar values of barotropic conversion relative to those of the reanalysis. However, for the summer months, positive values of CK are produced in excess when compared with those of reanalysis. Thus, the models would be producing stronger disturbances than observed.

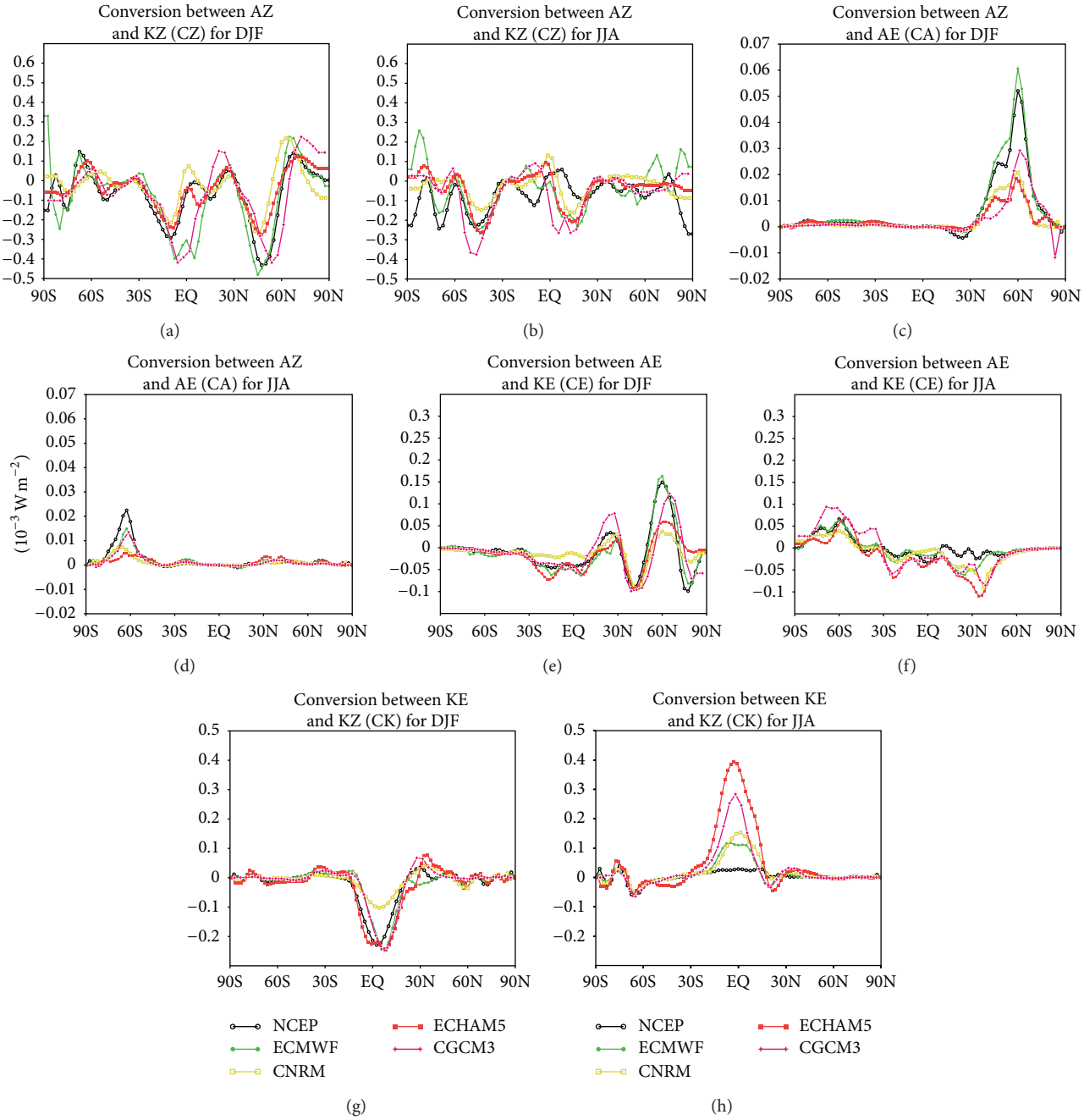

Figure 5: Latitudinal distribution of volume integrated conversion between AZ and KZ (CZ) for DJF (a) and JJA (b), conversion between AZ and AE (CA) for DJF (c) and JJA (d), conversion between AE and KE (CE) for DJF (e) and JJA (f), and conversion between KE and KZ (CK) for DJF (g) and JJA (h) averaged for the period from 1979 to 1999. Units are $\mathrm{Wm^{-2}}$.

3.3. The Energy Cycle Based on SRES-A2 Scenario. Sections 3.3 and 3.4 explore how the models characterize the energetics for the future climate. From the results of Sections 3.1 and 3.2 we know that the chosen models do a good job in reproducing the overall features of the energy conversions compared to the reanalysis, with a tendency to overestimate the zonal component of the circulation. This behavior needs to be taken into account when exploring future climate scenarios, so that this intrinsic bias is kept in proportion while assessing the future climate with the respective global energy changes.

In this section, we investigate details about the energy terms for the 1979–1999 (hereafter referred to as 20C3M) and 2079–2099 (SRES-A2 coupled models) periods. Figure 6 shows the annual climatological latitudinal distribution of the energy components along with their zonal and eddy components. The "error bars" (i.e., the inherent variability), indicating the 95% confidence level about the mean, are

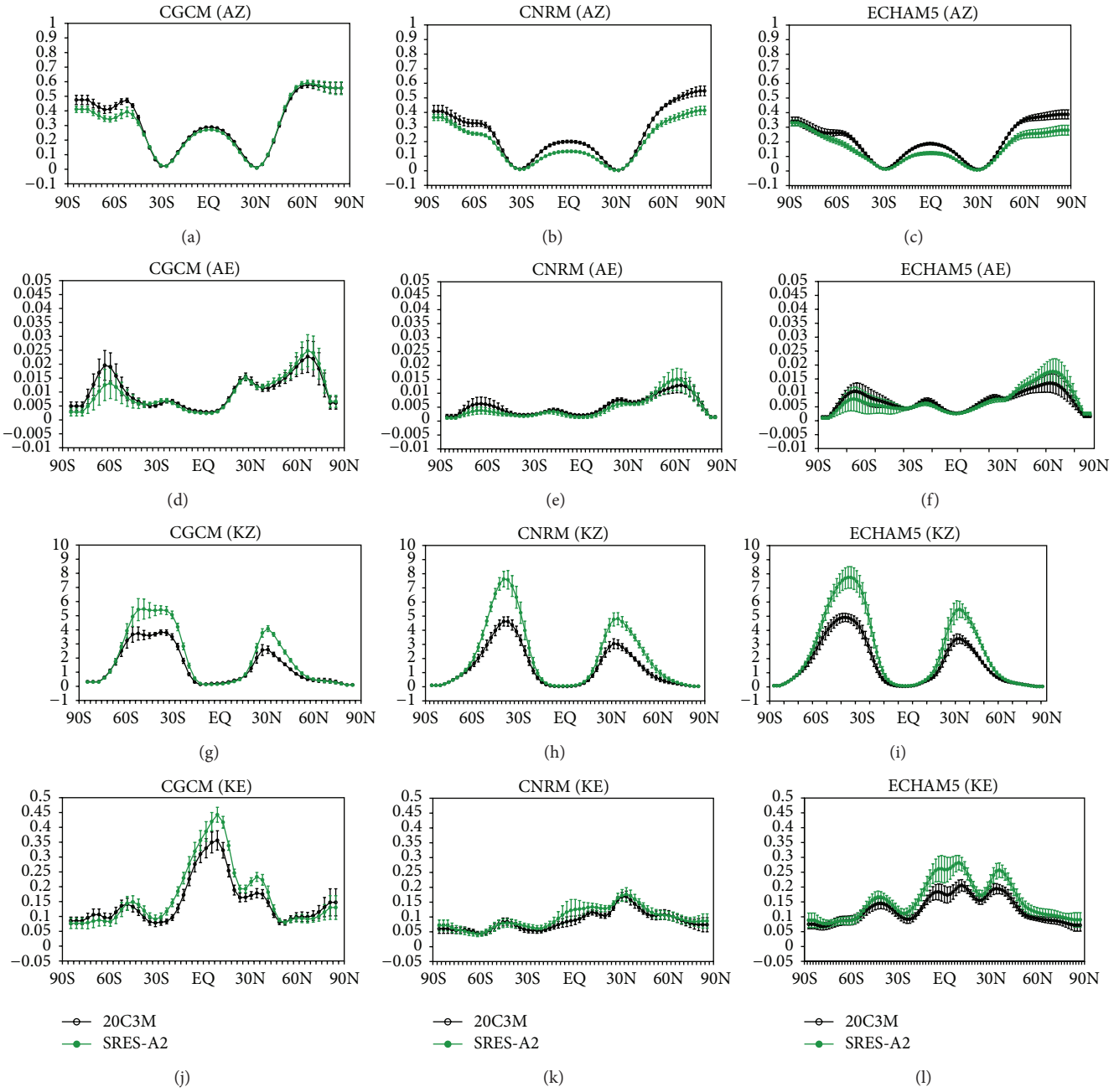

Figure 6: Annual latitudinal distribution of volume integrated of zonal available potential energy for CGCM (a), CNRM (b), and ECHAM5 (c), eddy available potential energy for CGCM (d), CNRM (e), and ECHAM5 (f), zonal kinetic energy for CGCM (g), CNRM (h), and ECHAM5 (i), and eddy kinetic energy for CGCM (j), CNRM (k), and ECHAM5 (l) models. Error bars indicate 95% confidence intervals about the mean. Units are 10^5 Jm^{-2}.

included in this panel to show the interannual variation experienced by the AZ term in each latitude belt. Figures 6(a)–6(c) show a decrease in zonal available potential energy for SRES-A2 in relation to 20C3M in almost all latitudes. The main statistically significant differences are observed at high latitudes of NH (Figures 6(b) and 6(c)). In the tropics and SH high latitudes the projected values of zonal available potential energy are also smaller than those produced during the 20C3M period, particularly for the CNRM and ECHAM5 models. The eddy component of available potential energy is shown in Figures 6(d)–6(f). These Figures show a small increase of eddy available potential energy around 60°N and a small decrease of this term in SH high latitudes for the SRES-A2 period. In the tropics there is no expressive difference between SRES-A2 and 20C3M. Figures 6(g)–6(i) show that the zonal kinetic energy significantly increases in a warmer climate, and this is maximized in the jet stream latitudes. The eddy component of kinetic energy also increases under

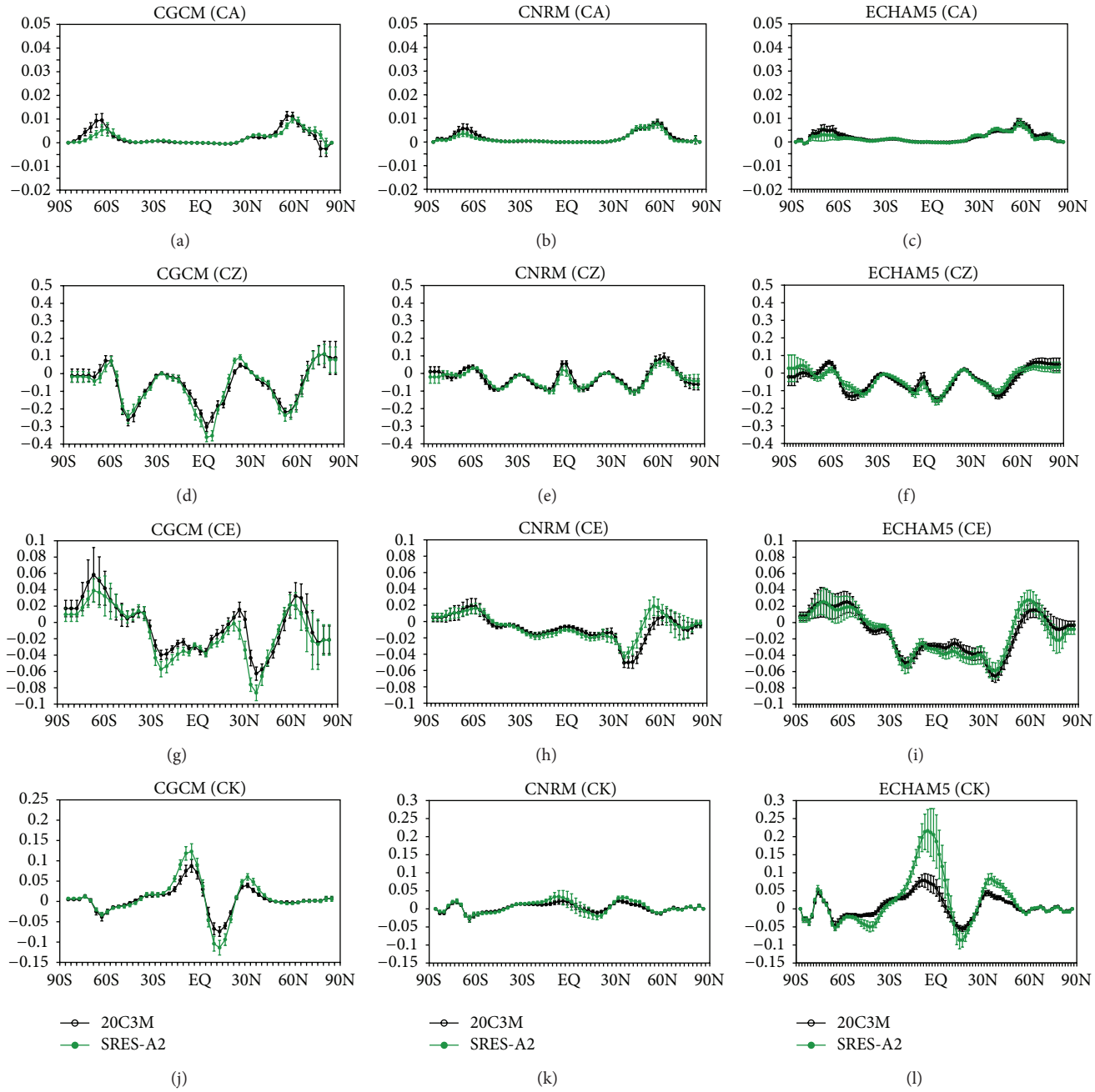

Figure 7: Latitudinal distribution of volume integrated of CA for CGCM (a), CNRM (b), and ECHAM5 (c), CZ for CGCM (d), CNRM (e), and ECHAM5 (f), CE for CGCM (g), CNRM (h), and ECHAM5 (i), and CK for CGCM (j), CNRM (k), and ECHAM5 (l) models. Error bars indicate 95% confidence intervals about the mean. Units are Wm^{-2}.

a warmer climate as seen from Figures 6(j)–6(l). However, significant changes occur just in restricted latitudes depending on the model. For example, significant changes around tropical latitudes are observed from CGCM and ECHAM5 models. The CGCM3 model shows a large increase in the tropical region, with a slight decrease of KE poleward of 60° in both hemispheres. The ECHAM5 and CNRM models do not produce a very marked peak over the tropics; however, they yield proportionally more eddy kinetic energy towards the subtropics.

The behavior of the conversion terms for both 20C3M and SREAS conditions is examined in Figure 7. Figures 7(a)–7(c) show that the latitudinal distribution of conversion between zonal and eddy available potential energy presents two positive peaks: one strong around 60°N and one less intense near 60°S for the 20C3M period. In the NH, CA is found between 30°N and high latitudes, while high values of CA in the SH are limited to high latitudes. All models reproduce well the latitudinal variability pattern. The results for SRES-A2 reveal a weakening of CA consistent with

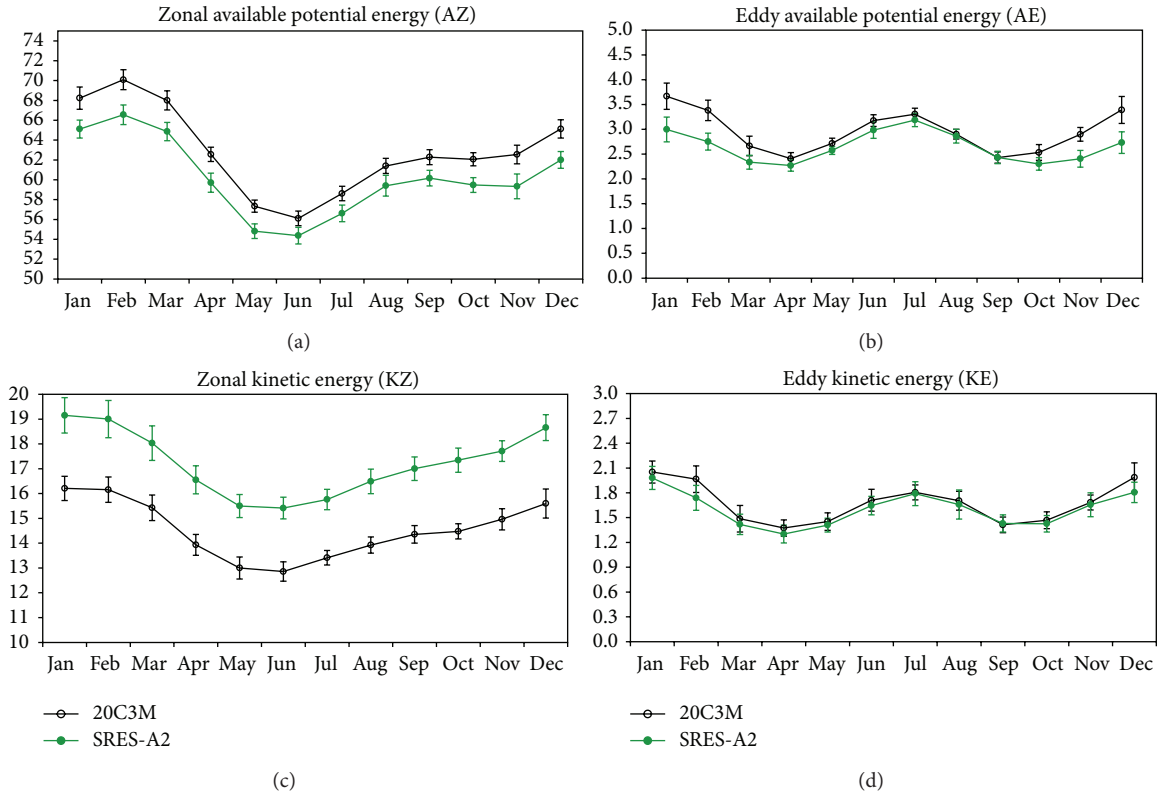

Figure 8: Mean SDLEC energy terms for the period 1979–1999 (20C3M) and 2079–2099 (SRES-A2). Results for 20C3M and SREAS2 are based on an average from CGCMs results (CRNM, CGCM, and ECHAM5). Error bars indicate 95% confidence intervals about the mean. Units are 10^5 Jm^{-2}.

less generation of eddy available potential energy, implying smaller disturbances on average. Small differences between CZ values are observed between the current climate and the SRES-A2 projection, as can be seen in Figures 7(d)–7(f). The baroclinic conversion differences from model to model can be seen in Figures 7(g)–7(i). CGCM3 shows a decrease in CE, especially in the subtropics (Figure 7(g)). CNRM shows an increase of CE between 30° and 60°N under SRES-A2, with a small decrease in the tropical region (Figure 7(h)). The same pattern is observed in the values of CE from ECHAM5 (Figure 7(i)). According to the CGCM3 model, there are an increase of barotropic conversion in the tropical region of the SH and a negative increase around 15 degrees in the Northern Hemisphere (Figure 7(j)). The ECHAM5 also shows a similar behavior, suggesting more available energy for the maintenance of blocking episodes in the subtropics under a warming scenario. This result agrees with earlier findings by the authors in [34] who showed longer lasting (although weaker) blocking occurrence under a doubled global CO_2 scenario.

3.4. Climatological Means of SDLEC for SRES-A2. The average annual cycle for a composite of model results for the 20C3M and SRES-A2 climate conditions is displayed in Figure 8. The error bars, indicating the 95% confidence level about the mean, are included in this panel to show the interannual variation experienced by the reservoir terms. The results show that both values of zonal and eddy available potential energy significantly diminish in a warming environment along the year (Figures 8(a) and 8(b)). The reduction in these quantities is related, respectively, to the weakening of meridional and zonal temperature contrasts in the atmosphere and suggests that less potential energy is available to be converted into zonal and eddy flow via CZ and CE conversion terms. The values of KZ are indicative of a much stronger zonal flow, for example, mid latitude and polar jet streams, in a warmer environment (Figure 8(c)). The values of KE are slightly, and nonstatistically significant, reduced in the SRES-A2 climate. Such a small difference between KE from 20C3M and SRES-A2 is due the low values of AE (Figure 8(b)) and CE (Figure 9(c)). The energy terms CA and CZ are significantly reduced in the SRES-A2 simulation, suggesting that less energy will be converted between AZ and AE and AZ and KZ (Figures 9(a) and 9(b)). This pattern is a consequence of the reduction in the AZ energy reservoir, as can be seen in Figure 8(a). Figures 9(c) and 9(d) show the annual cycle of both CE and CK for 20C3M and SRES-A2.

An interesting point is that, as it is observed in Figure 9, all energy conversion terms experience a decrease in the SRES-A2 simulation when compared with those in the 20C3M. The most significant are observed to occur during January to April and from November to December in CA

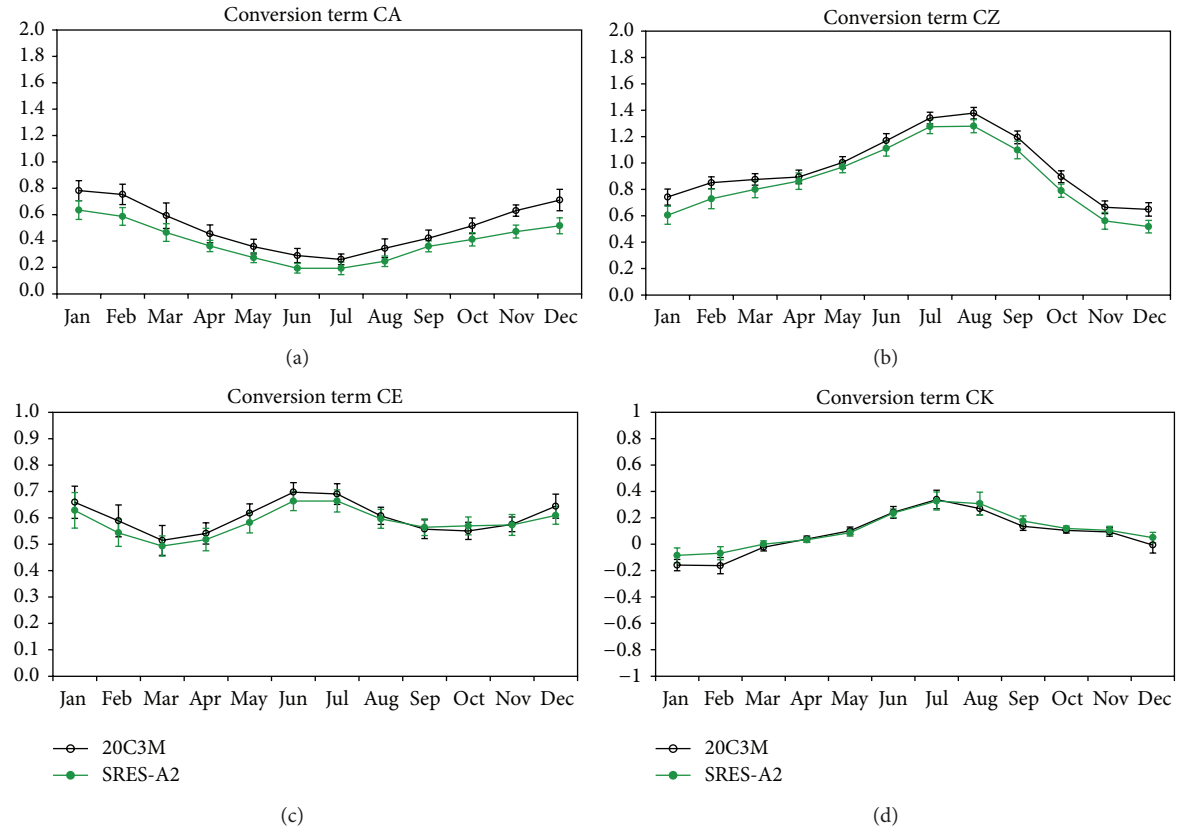

Figure 9: Mean SDLEC conversion terms for the period 1979–1999 (20C3M) and 2079–2099 (SRES-A2). Results for 20C3M and SREAS2 are based on an average from CGCMs results (CRNM, CGCM, and ECHAM5). Error bars indicate 95% confidence intervals about the mean. Units are Wm^{-2}.

term. The remaining conversion terms do not show statistically significant changes. In an anomaly perspective, the SDLEC flow is completely reversed, which is indicative of a significant change of the global atmospheric dynamics.

Model ensemble meridional distribution of energy and conversion for 20C3M and SRES-A2 are depicted in Figures 10(a)–10(d) and Figures 11(a)–11(d). The results suggest that in a warm climate, based on A2 CO_2 emission scenario, the zonal available potential energy is significantly reduced in low latitudes, limited by 15°S and 15°N, and at high latitudes (Figure 10(a)). Latitudinal mean values of AE show an increase in middle and high latitudes in the NH and decrease around 60°S (Figure 10(b)). Figures 10(c) and 10(d) show an increase of KZ and KE in the SRES-A2 period relative to the present climate, with significant changes in KZ. KZ values increase in both hemispheres and over regions where jet streams are climatologically observed. The rising of KE occurs in the tropics and NH subtropics. Annual latitudinal mean values of conversion terms are depicted in Figures 11(a)–11(d). As can be seen from Figure 11(a), the values of CA around 60°S for SRES-A2 are reduced when compared with those for 20C3M period. This reduction in CA values over these regions indicates a reduction in the change of energy between AZ and AE. Both CZ and CE terms do not show significant changes. However, CK values increase in tropical regions, limited by the latitudes of 30°S and 30°N. The increasing of CK values in the tropical regions points to a possible strengthening of large-scale disturbances via barotropic processes.

In order to evaluate the robustness of coupled models in reproducing the Lorenz energetics for the SRES-A2 forcing, Figure 12 compares the SDLEC for an average of reanalysis and coupled models. As can be noted from Figure 12(a), the values of AZ and KZ energy reservoirs are higher in models than in reanalyses, with AE being higher for the reanalysis ensemble and KE approximately keeping the same values for the reanalysis and coupled models. Both sets of values show GZ acting as source of energy to AZ, with the models producing the highest values. The values of eddy component of generation term show GE acting as a sink of energy for both reanalysis and GCMs. These results are consistent with [30], in which the authors explained the stronger energy cycle in the climate models related to reanalysis with generating push and dissipation pull hypothesis. They used such hypothesis to explain the high values of KZ and the low values of KE in the models. Accordingly, to them the excess of KZ is due to large values of AZ, with excessive DE (dissipation of eddy kinetic energy) producing lower values of KE compared to observations. The differences between the values of residuals of dissipation do not exceed 5%. The conversion fluxes flow from both sets of ensembles are in the same direction, with coupled models producing the highest values of CA, CE, and

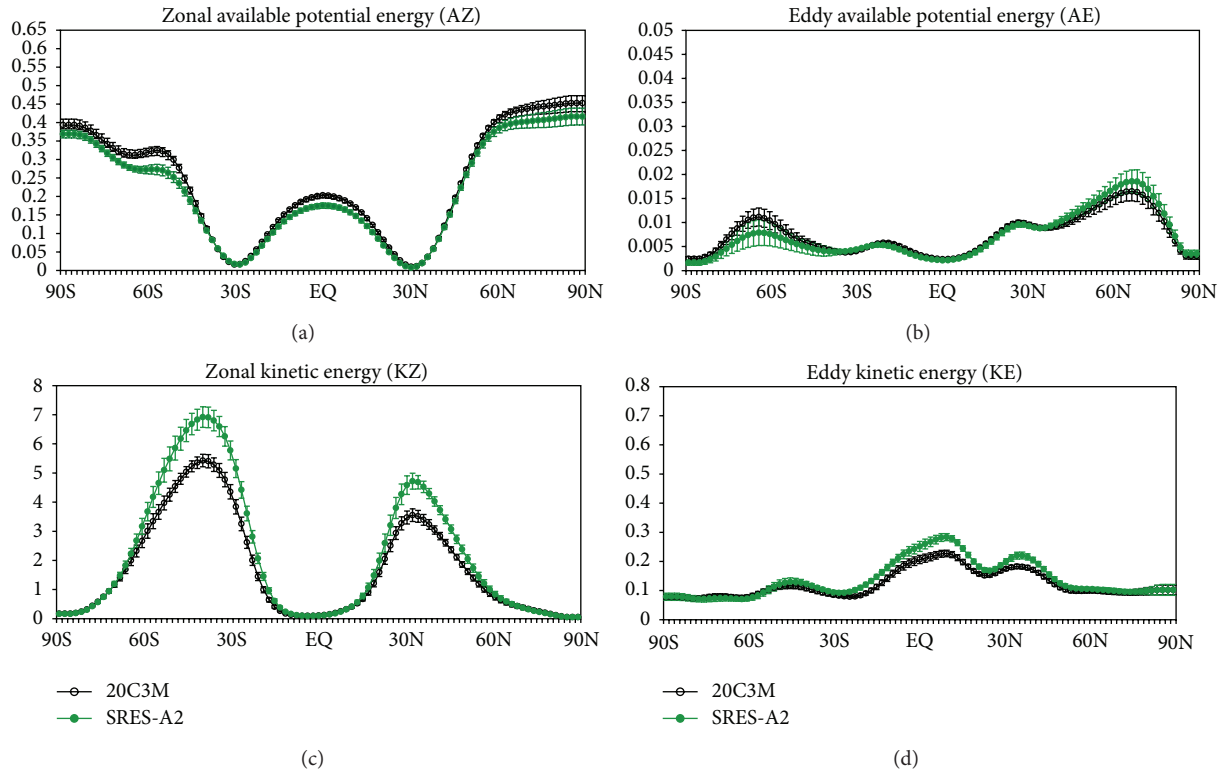

Figure 10: Annual latitudinal distribution of AZ (a), AE (b), KZ (c), and KE (d) for the 20C3M and SRES-A2 periods from an ensemble of models. Error bars indicate 95% confidence intervals about the mean. Units are 10^5 Jm^{-2}.

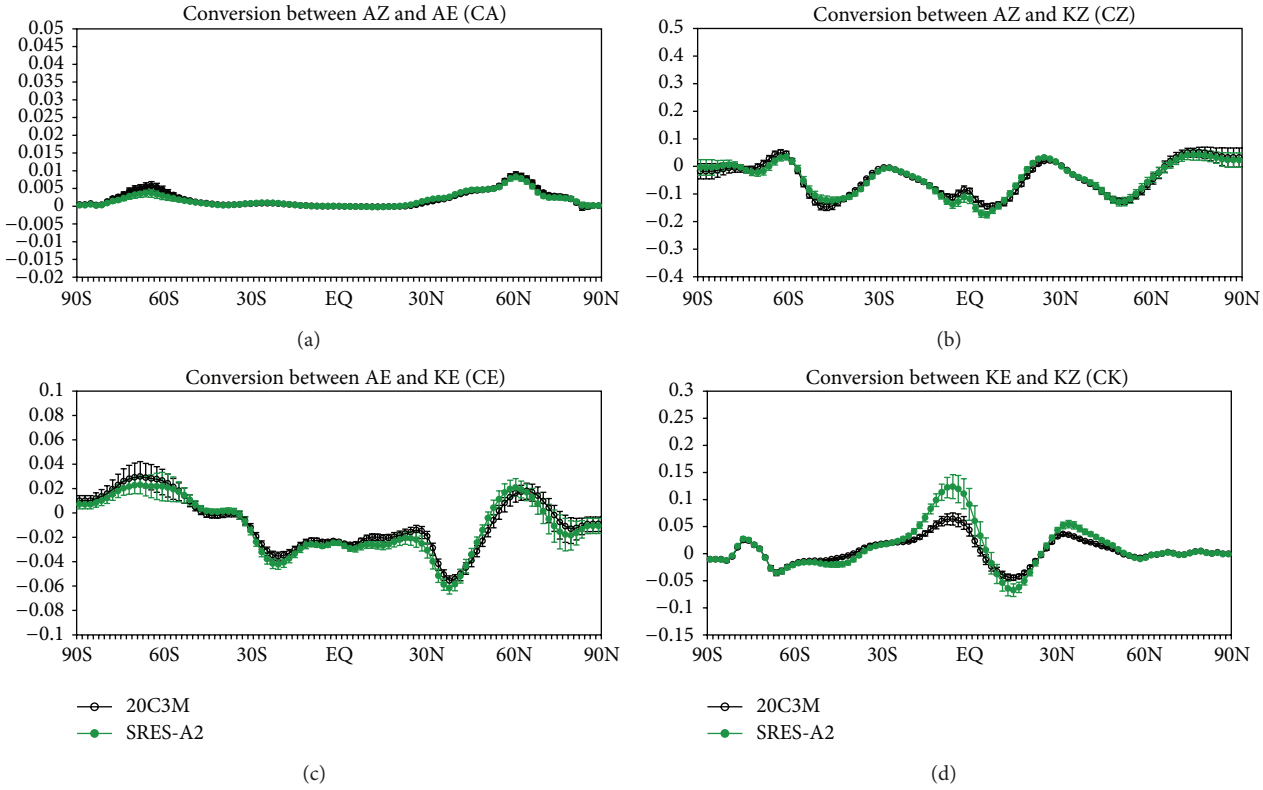

Figure 11: Annual latitudinal distribution of CZ (a), CA (b), CE (c), and CK (d) for the 20C3M and SRES-A2 periods from an ensemble of models. Error bars indicate 95% confidence intervals about the mean. Units are Wm^{-2}.

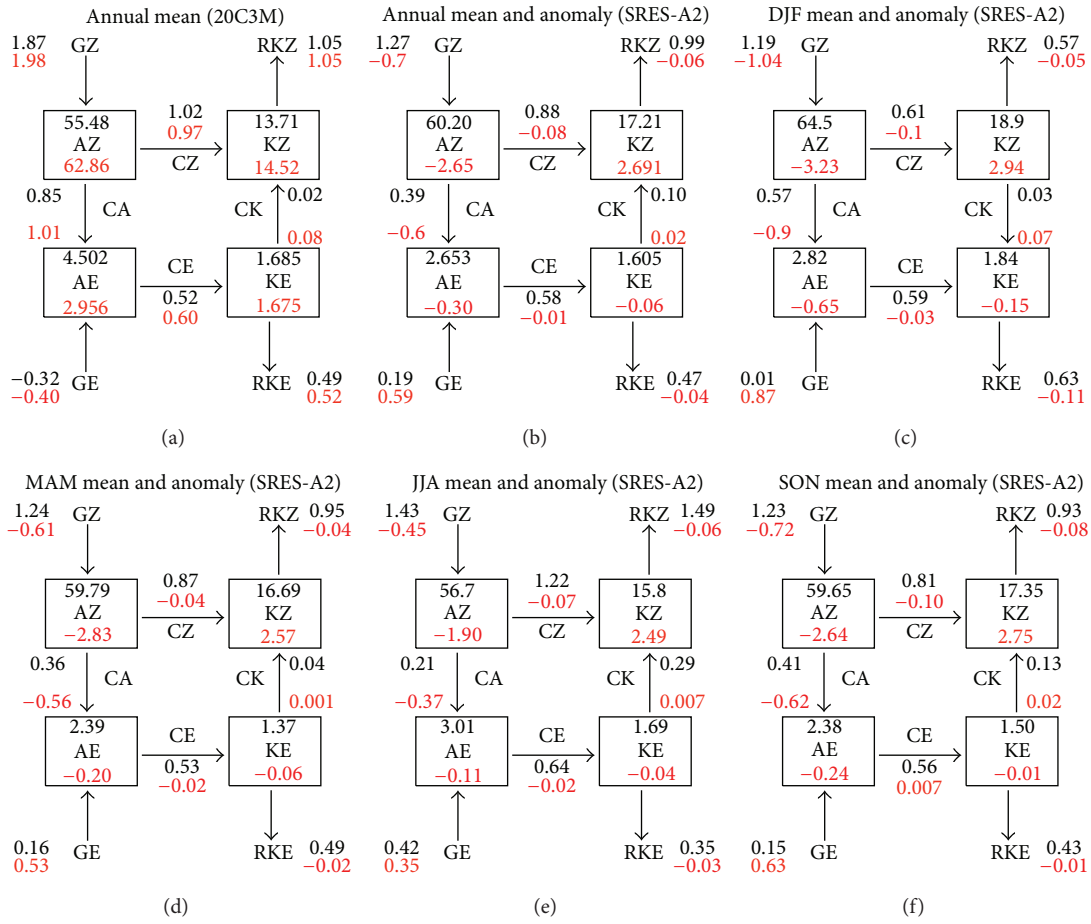

FIGURE 12: (a) Representation of the annual mean of SDLEC for an ensemble of reanalyses (black) and CGCMs (red) relative to 20C3M, (b) annual mean SDLEC for the ensemble of CGCMs (black) and anomaly (red) for the period of 2079–2099 (c). Panels (c), (d), (e), and (f) are representative SDLEC, respectively, for DJF, MAM, JJA, and SON seasons for the period of 2079–2099. Standard units are 10^5 Jm^{-2} and Wm^{-2}, respectively, for energy and conversion term.

CK. In an integrated perspective, that is, summing the eddy and zonal-average quantities (generation, available potential energy and dissipation process), and CZ and CE (not shown), coupled models exceed the generation, available potential energy, conversion between available potential energy and kinetic energy, and dissipation process, respectively, in 11.5%, 9.7%, 1.6%, 5.2%, and 1.6%. These results further reveal that even for higher values of generation, potential energy and kinetic energy in the coupled models, the growth of kinetic energy by the potential source (the conversion term, CZ + CE) remains approximately unchanged. This is possible under the consideration that the covariance between vertical velocity and absolute air temperature (for eddy and zonal-mean components) in both sets of ensembles is equivalent. Furthermore, these results suggest that the global SDLEC strength, which can be estimated from the conversion between potential energy and kinetic energy, is near the same for both sets of ensembles.

Figure 12(b) shows the values of annual mean SDLEC produced by the ensemble of coupled models for SRES-A2 forcing (color in black) and their respective anomalies, measured by the difference between the coupled model ensemble in the period of 20C3M and SRES-A2 CO_2 in red. It can be seen that in a high CO_2 concentration environment higher anomalies are observed in zonal energy reservoirs than in their eddy components. Both zonal and eddy available potential energies are reduced in the SRES-A2 projection, while kinetic energy increases mainly in the zonal component. Reduction is observed in the total conversion between potential energy and kinetic energy (CZ + CE), followed by an increase of 24.2% in the barotropic conversion term (CK). These results are indicative of the anomalous increase of KZ that comes from the anomalous rising in CK, as CZ decreases. These findings are in agreement with [32, 35] results, which found significant reduction in the main components of the energy cycle for a CO_2 atmospheric concentration doubled condition.

The reduction of AZ, in the SRES-A2 environment, must be related in part to the decrease of 20.2% in zonal-mean generation of potential energy (GZ), as a consequence of the weakening of meridional temperature in the atmosphere due to positive temperature anomalies in high levels over

the tropics and in the lower troposphere in polar regions [36]. This reduction in AZ provoked a reduction in both CA and CZ, respectively, of 15.5% and 9.0%. The reduction in the values of baroclinic term (CE) is not significant, suggesting that in a global sense the departures of kinetic energy from the kinetic zonal-mean do not represent an anomalous growth at the expense of AE. The results still show a small reduction in the residual dissipation terms. Figures 12(c)–12(f) show the seasonal climatological values of SDLEC. For all seasons the negative anomaly in AZ, AE, and KE still persists, followed by positive anomalous KZ. The same behavior is observed in GZ, RKZ, RKE, and GE, when compared to the annual mean. For all seasons the energy and conversion terms, including residual dissipation and generation terms, are given by negative anomalies, with maximum total potential and kinetics energy (AZ + AE and KZ + KE), conversion from potential to kinetic energy (CZ + CE), and residual dissipation term (RKZ + RKE) in DJF. Their corresponding anomalies for SRES-A2 are also higher in this season.

4. Summary

The present study carried out a global energy analysis in order to quantify the differences between the period 1979–1999 and the period 2079–2099 under the SRES-A2 CO_2 forcing condition. The energy results of three coupled climate models are compared to NCEP-II and ERA-40 reanalyses for the period from 1979 to 1999 as a validation point. The energetic changes are achieved by computing the anomalies between the ensemble of coupled models for the two periods of analysis. The analysis of the energetic results is divided into time series, latitudinal distribution and volume integrated based on SRES-A2 forcing.

Averaged monthly means of energy and conversion terms were carried out for the period from 1979 to 1999 from reanalysis data and coupled model data. Results for energy and conversion terms from both reanalysis are very similar in terms of magnitude and month to month variation. GZ is higher in winter, while maximum values of GE occur over the summer months. The three coupled models used in this study adequately simulate the seasonal behavior of both types of generation of available potential energy. The coupled models yield more zonal available potential energy compared to observed values. Although the models are able to produce phase and amplitude of AE, they systematically underestimate its magnitude. Less production of AE by the coupled models can reflect into a slower growing of eddy disturbances via baroclinic process and/or a redirection of energy to GE and AZ components of the energy cycle. The models ECHAM5 and CGCM3 produce values of KZ higher than those of the reanalysis. The maximum values of CZ produced by the reanalysis for summer are well simulated by the coupled models. Furthermore, climatologically the values of CZ are indicative of an energy flow directed from AZ to KZ, which was verified by the models. The climate models adequately reproduce the annual cycle of CA, CE, and CK in a general sense.

The latitudinal distribution of energy and conversion terms for the period from 1979 to 1999 has shown that coupled models are able to simulate reasonably well the meridional variations of AZ for both summer and winter, including the phase and amplitude of AZ values. The largest values of AZ are observed from mid to high latitudes during summer in both hemispheres. The highest value of AE as observed from reanalysis is located around 60° N during winter, with CNRM and ECHAM5 simulating low values of AE at this latitude. The CNRM model reproduced well the meridional variations of AE. Significant discrepancies between both reanalysis and coupled models relative to KZ values were noted. Excessive values of KZ are produced by the coupled models relative to reanalysis in both hemispheres. The ECHAM5 and CNRM almost double the values of KZ in the SH. However, the CGCM3 gives values and meridional distribution similar to those of the reanalysis. Furthermore, the ECHAM5 and CNRM models were unable to simulate the double jet structure in the SH. For the case of eddy zonal kinetic energy, it was observed that the values of KE from coupled models are consistently lower than those produced by ERA-40 and NCEP-II. It was also observed that the coupled models underestimate the values of KE in NH high latitudes.

Time series of a composite of models show that both zonal and eddy available potential energies decrease in a warmer environment for all seasons. These reductions suggest that less potential energy is available to be converted into zonal and eddy flow via CZ and CE. Positive anomalies of KZ and negative anomalies of KE suggest an increase in the mid latitude jet stream and a reduction in the intensity of the eddies under increased CO_2 condition. A revealing point is that all the values of energy conversion terms decrease in SRES-A2 climate when compared with those in the 20C3 M period. Reduction is still observed in the total conversion between available potential energy and kinetic energy, followed by a 24.2% increase in the barotropic term. It is observed that the reduction of AZ is due the diminishing of GZ in the SRES-A2 forcing period. This induced reduction induces a decrease in both CA and CZ. No significant change in the baroclinic conversion term is observed. Therefore anomalous SDLEC relative to the 20C3M climate depicts an overall reduction in the strength of global energetics in the energy flows.

Our results contribute towards a better understanding of the variability and evolution of the global energetics, further validating and complementing the recent works of [24, 33] under the perspective of our explicit calculation of the eddy component in the energy equations. The range of IPCC models used in our analyses confirms the overall traits first found by [24], increasing our confidence in how the energetics will respond to further increases in the global temperature. Our analyses also provide for the first time guidance into how the energy generation terms are compared with the reanalyses, highlighting that the models tend to have a reduced ability to generate potential energy compared to the reanalysis particularly during the northern winter. However, over the southern winter, the eddy potential energy is stronger in the models, suggesting that the models can reproduce the transient activity better in the Southern

Hemisphere. The reasons for this behaviour are currently being investigated.

Appendix

Lorenz Energetics

Equations of Lorenz in Spatial Domain: Mathematical Expression of Components in the Energy Balance (1)-(4). The zonal mean of a variable X between longitudes λ_1 and λ_2 is given by

$$[X]_\lambda = \frac{1}{\lambda_2 - \lambda_1} \int_{p_1}^{p_2} X \, d\lambda. \tag{A.1}$$

The eddy component of this variable is

$$(X)_\lambda = X - [X]_\lambda. \tag{A.2}$$

The mean of X over an area bounded by longitudes λ_1 and λ_2 and latitudes ϕ_1 and ϕ_2 is

$$[X]_{\lambda\phi} = \frac{1}{\lambda_2 - \lambda_1} \frac{1}{\sin\phi_2 - \sin\phi_1} \int_{\phi_1}^{\phi_2} \int_{\lambda_1}^{\lambda_2} X \cos\phi \, d\lambda \, d\phi. \tag{A.3}$$

Defining the quantity

$$([X]_\lambda)_\phi = [X]_\lambda - [X]_{\lambda\phi}, \tag{A.4}$$

the four energy forms in the SDLEC are

$$\begin{aligned}
\mathrm{AZ} &= \int_{p_1}^{p_2} \frac{\left[([T]_\lambda)_\phi^2\right]_{\lambda\phi}}{2[\sigma]_{\lambda\phi}} \, dp, \\
\mathrm{AE} &= \int_{p_1}^{p_2} \frac{\left[(T)_\lambda^2\right]_{\lambda\phi}}{2[\sigma]_{\lambda\phi}} \, dp, \\
\mathrm{KZ} &= \int_{p_1}^{p_2} \frac{\left[[u]_\lambda^2 + [v]_\lambda^2\right]_{\lambda\phi}}{2g} \, dp, \\
\mathrm{KE} &= \int_{p_1}^{p_2} \frac{\left[(u)_\lambda^2 + (v)_\lambda^2\right]_{\lambda\phi}}{2g} \, dp,
\end{aligned} \tag{A.5}$$

where p_1 and p_2 are, respectively, the upper and lower pressure boundaries, T is the temperature, g is the magnitude of the acceleration of gravity, u and v are the eastward and northward components of the wind, respectively, and σ is the static stability parameter which is given by

$$\begin{aligned}
[\sigma]_{\lambda\phi} &= \left[\frac{gT}{c_p} - \frac{gp}{R}\frac{\partial T}{\partial p}\right]_{\lambda\phi}, \\
\mathrm{CZ} &= \int_{p_1}^{p_2} -\left[([\omega]_\lambda)_\phi([T]_\lambda)_\phi\right]_{\lambda\phi} \frac{R}{gp} dp, \\
\mathrm{CE} &= \int_{p_1}^{p_2} -\left[(\omega)_\lambda(T)_\lambda\right]_{\lambda\phi} \frac{R}{gp} dp, \\
\mathrm{CA} &= \int_{p_1}^{p_2} -\Bigg(\left[\frac{(v)_\lambda(T)_\lambda}{2[\sigma]_{\lambda\phi} r} \frac{\partial([T]_\lambda)}{\partial\phi}\right]_{\lambda\phi} \\
&\qquad + \left[\frac{(\omega)_\lambda(T)_\lambda}{p^{R/c_p}} \frac{\partial}{\partial p} \right. \\
&\qquad \left. \times \left(\frac{([T]_\lambda)_\phi p^{R/c_p}}{[\sigma]_{\lambda\phi}}\right)\right]_{\lambda\phi} \Bigg) dp, \\
\mathrm{CK} &= \int_{p_1}^{p_2} \frac{1}{g}\left[(v)_\lambda(u)_\lambda \frac{\cos\phi}{r} \frac{\partial}{\partial\phi}\left(\frac{[u]_\lambda}{\cos\phi}\right)\right]_{\lambda\phi} dp \\
&\quad + \int_{p_1}^{p_2} \frac{1}{g}\left[\frac{(v)_\lambda^2}{r}\frac{\partial[v]_\lambda}{\partial\phi}\right]_{\lambda\phi} dp \\
&\quad + \int_{p_1}^{p_2} \frac{1}{g}\left[[v]_\lambda(u)_\lambda^2 \frac{\tan\phi}{r}\right]_{\lambda\phi} dp \\
&\quad - \int_{p_1}^{p_2} \frac{1}{g}\left[(\omega)_\lambda(u)_\lambda \frac{\partial[u]_\lambda}{\partial p}\right]_{\lambda\phi} dp \\
&\quad + \int_{p_1}^{p_2} \frac{1}{g}\left[(\omega)_\lambda(v)_\lambda \frac{\partial[v]_\lambda}{\partial p}\right]_{\lambda\phi} dp,
\end{aligned} \tag{A.6}$$

where r denotes the mean radius of the earth.

The generation of APE terms and kinetic energy dissipation terms is

$$\begin{aligned}
\mathrm{GZ} &= \int_{p_1}^{p_2} \frac{\left[([q]_\lambda)_\phi([T]_\lambda)_\phi\right]_{\lambda\phi}}{c_p[\sigma]_{\lambda\phi}} dp, \\
\mathrm{GE} &= \int_{p_1}^{p_2} \frac{\left[(q)_\lambda[T]_\lambda\right]_{\lambda\phi}}{c_p[\sigma]_{\lambda\phi}} dp,
\end{aligned} \tag{A.7}$$

where q denotes the diabatic processes associated with the generation of APE.

The energy transport integrals are

$$\begin{aligned}
\mathrm{BAZ} = c_1 &\int_{p_1}^{p_2}\int_{\lambda_1}^{\lambda_2} \frac{1}{2\,[\sigma]_{\lambda\phi}}\Big(2\,([T]_\lambda)_\phi (T)_\lambda u \\
&\qquad + ([T]_\lambda)_\phi^2 u\Big)_{\lambda_1}^{\lambda_2} d\phi\, dp \\
&+ c_2 \int_{p_1}^{p_2} \frac{1}{2\,[\sigma]_{\lambda\phi}}\Big(2[(v)_\lambda (T)_\lambda]_\lambda ([T]_\lambda)_\phi \cos\phi \\
&\qquad + ([T]_\lambda)_\phi^2 [v]_\lambda \cos\phi\Big)_{\phi_1}^{\phi_2} dp \\
&- \frac{1}{2[\sigma]_{\lambda\phi}}\Big(\big[2(\omega)_\lambda (T)_\lambda\big]_\lambda ([T]_\lambda)_\phi \\
&\qquad + \big[[\omega]_\lambda ([T]_\lambda)_\phi^2\big]_{\lambda\phi}\Big)_{p_1}^{p_2}, \\
\mathrm{BAE} = c_1 &\int_{p_1}^{p_2}\int_{\phi_1}^{\phi_2} \frac{1}{2[\sigma]_{\lambda\phi}}\big[u(T)_\lambda^2\big]_{\lambda_1}^{\lambda_2} d\phi\, dp \\
&+ c_2 \int_{p_1}^{p_2} \frac{1}{2[\sigma]_{\lambda\phi}}\Big(\big[(T)_\lambda^2\big]_\lambda \cos\phi\Big)_{\phi_1}^{\phi_2} dp \\
&- \left(\frac{\big[\omega(T)_\lambda^2\big]_{\lambda\phi}}{2[\sigma]_{\lambda\sigma}}\right)_{p_1}^{p_2}, \\
\mathrm{BKZ} = c_1 &\int_{p_1}^{p_2}\int_{\phi_1}^{\phi_2} \frac{1}{2g}\Big(u\big[u^2 + v^2 - (u)_\lambda^2 - (v)_\lambda^2\big]\Big)_{\lambda_1}^{\lambda_2} d\phi\, dp \\
&+ c_2 \int_{p_1}^{p_2} \frac{1}{2g}\Big(\big[v\cos\phi\,\big[u^2 + v^2 - (u)_\lambda^2\big]\big]_\lambda\Big)_{\phi_1}^{\phi_2} dp \\
&- \left(\frac{1}{2g}\big[\omega\,\big[u^2 + v^2 - (u)_\lambda^2 - (v)_\lambda^2\big]\big]_{\lambda\phi}\right)_{p_1}^{p_2}, \\
\mathrm{BKE} = c_1 &\int_{p_1}^{p_2}\int_{\phi_1}^{\phi_2} \frac{1}{2g}\Big(u\big[(u)_\lambda^2 + (v)_\lambda^2\big]\Big)_{\lambda_1}^{\lambda_2} d\phi\, dp \\
&+ c_2 \int_{p_1}^{p_2} \frac{1}{2g}\Big(\big[v\cos\phi\,\big[(u)_\lambda^2 + \big((v)_\lambda^2\big)\big]\big]_\lambda\Big)_{\phi_1}^{\phi_2} dp \\
&- \left(\frac{1}{2g}\big[\omega\,\big[(u)_\lambda^2 + (v)_\lambda^2\big]\big]_{\lambda\phi}\right)_{p_1}^{p_2},
\end{aligned} \tag{A.8}$$

where $c_1 = -[r(\lambda_2 - \lambda_1)(\sin\phi_2 - \phi_1)]^{-1}$ e $c_2 = -[r(\sin\phi_2 - \phi_1)]^{-1}$.

Finally the integrals for BΦZ and BΦE are

$$\begin{aligned}
\mathrm{B\Phi Z} = c_1 &\int_{p_1}^{p_2}\int_{\phi_1}^{\phi_2} \frac{1}{g}\Big([v]_\lambda ([\Phi]_\lambda)_\phi\Big)_{\lambda_1}^{\lambda_2} d\phi\, dp \\
&+ c_2 \int_{p_1}^{p_2} \frac{1}{g}\Big(\cos\phi[v]_\lambda ([\Phi]_\lambda)_\phi\Big)_{\phi_1}^{\phi_2} dp \\
&- \frac{1}{g}\Big(\big[([\omega]_\lambda)_\phi ([\Phi]_\lambda)_\phi\big]_{\lambda\phi}\Big)_{p_1}^{p_2},
\end{aligned} \tag{A.9}$$

$$\begin{aligned}
\mathrm{B\Phi E} = c_1 &\int_{p_1}^{p_2}\int_{\phi_1}^{\phi_2} \frac{1}{g}((u)_\lambda (\Phi)_\lambda)_{\lambda_1}^{\lambda_2} d\phi\, dp \\
&+ c_2 \int_{p_1}^{p_2} \frac{1}{g}\big([(v)_\lambda\,(\Phi)_\lambda]\cos\phi\big)_{\phi_1}^{\phi_2} \\
&- \frac{1}{g}\big([(\omega)_\lambda (\Phi)_\lambda]_{\lambda\phi}\big)_{p_1}^{p_2},
\end{aligned} \tag{A.10}$$

where $\Phi(= gz)$ is the geopotential.

Acknowledgments

José Augusto P. Veiga and Tercio Ambrizzi were supported by CNPq (150356/2011-0). Tercio Ambrizzi also has the support from the FAPESP (08/58101-9), CLARIS LPB, and INCLINE/USP. Alexandre B. Pezza would like to acknowledge the Australian Research Council (ARC) for funding parts of this work.

References

[1] E. Agee, "Trends in cyclone and anticyclone frequency and comparison with periods of warming and cooling over the northern hemisphere," *Journal of Climate*, vol. 4, pp. 263–267, 1991.

[2] J. Paciorek, S. Risbey, V. Ventura, and R. D. Rosen, "Multiple indices of Northern Hemisphere cyclone activity, winters 1949–1999," *Journal of Climate*, vol. 15, no. 13, pp. 1573–1590, 2002.

[3] B. Elsner, P. Kossin, and H. Jagger, "The increasing intensity of the strongest tropical cyclones," *Nature*, vol. 455, pp. 92–95, 2008.

[4] S. Solomon, D. Qin, M. Manning et al., *The Physical Science Basis. Contribution of Working Group I To the Fourth Assessment Report of the Intergovernmental Panel on Climate Change*, Cambridge University Press, Cambridge, UK, 2007.

[5] C. Serreze, F. Carse, G. Barry, and J. C. Rogers, "Icelandic low cyclone activity: climatological features, linkages with the NAO, and relationships with recent changes in the Northern Hemisphere circulation," *Journal of Climate*, vol. 10, no. 3, pp. 453–464, 1997.

[6] J. McCabe, C. Martyn, and C. Serreze, "Trends in Northern Hemisphere surface cyclone frequency and intensity," *Journal of Climate*, vol. 15, pp. 2763–2768, 2001.

[7] P. A. O'Gorman, "The effective static stability experienced by eddies in a moist atmosphere," *Journal of the Atmospheric Sciences*, vol. 68, no. 1, pp. 75–90, 2011.

[8] I. Simmonds and K. Keay, "Variability of Southern Hemisphere extratropical cyclone behavior," *Journal of Climate*, vol. 13, no. 3, pp. 550–561, 2000.

[9] E.-P. Lim and I. Simmonds, "Explosive cyclone development in the Southern Hemisphere and a comparison with Northern Hemisphere events," *Monthly Weather Review*, vol. 130, no. 9, pp. 2188–2209, 2002.

[10] A. B. Pezza and T. Ambrizzi, "Variability of Southern Hemisphere cyclone and anticyclone behavior: further analysis," *Journal of Climate*, vol. 16, pp. 1075–1083, 2003.

[11] A. B. Pezza, I. Simmonds, and A. Renwick, "Southern hemisphere cyclones and anticyclones: recent trends and links with decadal variability in the Pacific Ocean," *International Journal of Climatology*, vol. 27, no. 11, pp. 1403–1419, 2007.

[12] U. Neu, M. Akperov, and N. Bellenbaum, "IMILAST—a community effort to intercompare extratropical cyclone detection and tracking algorithms," *Bulletin of the American Meteorological Society*, vol. 94, no. 4, pp. 529–547, 2013.

[13] U. Ulbrich, G. Leckebusch, and J. Grieger, "Are greenhouse gas signals of Northern Hemisphere Winter extra-tropical cyclone activity dependen ton the identification and traking algorithm?" *Meteorologische Zeitschrift*, vol. 22, pp. 61–68, 2013.

[14] M. Sugi and M. Sato, "Influence of the global warming on tropical cyclone climatology: an experiment with the JMA global model," *Journal of the Meteorological Society of Japan*, vol. 80, no. 2, pp. 249–272, 2002.

[15] K. Emanuel, "Increasing destructiveness of tropical cyclones over the past 30 years," *Nature*, vol. 36, pp. 686–688, 2005.

[16] K. Oouchi, "Tropical cyclone climatology in a global-warming climate as simulated in a 20 km-mesh global atmospheric model: frequency and wind intensity analyses," *Journal of the Meteorological Society of Japan*, vol. 84, no. 2, pp. 259–276, 2006.

[17] D. Hoyos, A. Agudelo, J. Webster, and A. Curry, "Deconvolution of the factors contributing to the increase in global hurricane intensity," *Science*, vol. 312, no. 5770, pp. 94–97, 2006.

[18] E. N. Lorenz, "Available potential energy," *Tellus*, vol. 7, pp. 157–167, 1955.

[19] B. Saltsman, "Equations governing the energetics of the larger scales of atmospheric turbulence in the domain of wave number," *Journal of Meteorology*, vol. 14, pp. 513–523, 1957.

[20] A. Plumb, "A new look at the energy cycle," *Journal of the Atmospheric Sciences*, vol. 40, no. 7, pp. 1669–1688, 1983.

[21] J. Lambert, "The effect of enhanced greenhouse warming on winter cyclone frequencies and strengths," *Journal of Climate*, vol. 8, no. 5, pp. 1447–1452, 1995.

[22] T. Iwasaki, "Atmospheric energy cycle viewed from wave-mean-flow interaction and Lagrangian mean circulation," *Journal of the Atmospheric Sciences*, vol. 58, no. 20, pp. 3036–3052, 2001.

[23] S. Murakami, "Atmospheric local energetics and energy interactions between mean and eddy fields. Part I: theory," *Journal of the Atmospheric Sciences*, vol. 68, no. 4, pp. 760–768, 2011.

[24] D. Hernández-Deckers and S. von Storch, "Energetics responses to increases in greenhouse gas concentration," *Journal of Climate*, vol. 23, no. 14, pp. 3874–3887, 2010.

[25] M. Kanamitsu, W. Ebisuzaki, J. Woollen et al., "NCEP-DOE AMIP-II reanalysis (R-2)," *Bulletin of the American Meteorological Society*, vol. 83, no. 11, pp. 1631–1643, 2002.

[26] S. Uppala, W. Kayllberg, J. Simmonds et al., "The ERA-40 reanalysis," *Quarterly Journal of the Royal Meteorological Society*, vol. 131, pp. 2961–3012, 2005.

[27] E. Roeckner, R. Brokofp, M. Esch et al., "The atmospheric general circulation model ECHAM5. Part II: sensitivity of simulated climate to horizontal and vertical resolution," Tech. Rep. 349, 2004.

[28] F. Scinocca, A. McFarlane, M. Lazare, J. Li, and D. Plummer, "Technical note: the CCCma third generation AGCM and its extension into the middle atmosphere," *Atmospheric Chemistry and Physics*, vol. 8, no. 23, pp. 7055–7074, 2008.

[29] D. Salas-Mélia, F. Chauvin, M. Déqué et al., "Description and validation of the CNRM-CM3 global coupled model," CNRM Working Note 103, 2005.

[30] J. Boer and S. Lambert, "The energy cycle in atmospheric models," *Climate Dynamics*, vol. 30, no. 4, pp. 371–390, 2008.

[31] C. Marques, A. Rocha, J. Corte-Real, J. M. Castanheira, J. Ferreira, and P. Melo-Gonçalves, "Global atmospheric energetics from NCEP-Reanalysis 2 and ECMWF-ERA40 Reanalysis," *International Journal of Climatology*, vol. 29, no. 2, pp. 159–174, 2009.

[32] D. Hernández-Deckers and S. von Storch, "The energetics response to a warmer climate: relative contributions from the transient and stationary eddies," *Earth System Dynamics*, vol. 2, pp. 105–120, 2011.

[33] C. Marques, A. Rocha, and J. Corte-Real, "Global diagnostic energetics of five state-of-the-art climate models," *Climate Dynamics*, vol. 36, pp. 1767–1794, 2010.

[34] R. Lupo, J. Oglesby, and I. Mokhov, "Climatological features of blocking anticyclones: a study of Northern Hemisphere CCM1 model blocking events in present-day and double CO_2 concentration atmospheres," *Climate Dynamics*, vol. 13, no. 3, pp. 181–195, 1997.

[35] J. A. P. Veiga and T. Ambrizzi, "A global and hemispherical analysis of the Lorenz energetics based on the RepresentativeConcentration Pathways used in CMIP5," *Advances in Meteorology*. In press.

[36] J. Boer, "Some dynamical consequences of greenhouse gas warming," *Atmosphere*, vol. 33, no. 4, pp. 731–751, 1995.